Artificial Intelligence In Medicine 143 (2023) 102630

Contents lists available at ScienceDirect

Artificial Intelligence In Medicine

journal homepage: www.elsevier.com/locate/artmed

Research paper

Insight into ADHD diagnosis with deep learning on Actimetry: Quantitative interpretation of occlusion maps in age and gender subgroups

Patricia Amado-Caballero [a,*], Pablo Casaseca-de-la-Higuera [a], Susana Alberola-López [b], Jesús María Andrés-de-Llano [c], José Antonio López-Villalobos [c], Carlos Alberola-López [a]

[a] Laboratorio de Procesado de Imagen (LPI), Universidad de Valladolid, Valladolid, Spain
[b] Centro de Salud Jardinillos, 34001 Palencia, Spain
[c] Complejo Asistencial Universitario de Palencia, 34005 Palencia, Spain

ARTICLE INFO

Keywords:
ADHD
Actigraphy
Deep learning
Understandable AI

ABSTRACT

Attention Deficit/Hyperactivity Disorder (ADHD) is a prevalent neurodevelopmental disorder in childhood that often persists into adulthood. Objectively diagnosing ADHD can be challenging due to the reliance on subjective questionnaires in clinical assessment. Fortunately, recent advancements in artificial intelligence (AI) have shown promise in providing objective diagnoses through the analysis of medical images or activity recordings. These AI-based techniques have demonstrated accurate ADHD diagnosis; however, the growing complexity of deep learning models has introduced a lack of interpretability. These models often function as black boxes, unable to offer meaningful insights into the data patterns that characterize ADHD.

Objective: This paper proposes a methodology to interpret the output of an AI-based diagnosis system for combined ADHD in age and gender-stratified populations.

Methods: Our system is based on the analysis of 24 hour-long activity records using Convolutional Neural Networks (CNNs) to classify spectrograms of activity windows. These windows are interpreted using occlusion maps to highlight the time–frequency patterns explaining ADHD activity.

Results: Significant differences in the frequency patterns between ADHD and controls both in diurnal and nocturnal activity were found for all the populations. Temporal dispersion also presented differences in the male population.

Conclusion: The proposed interpretation techniques for CNNs highlighted gender- and age-related differences between ADHD patients and controls. Leveraging these differences could potentially lead to improved diagnostic accuracy, especially if a larger and more balanced dataset is utilized.

Significance: Our findings pave the way for the development of an AI-based diagnosis system for ADHD that offers interpretability, thereby providing valuable insights into the underlying etiology of the disease.

1. Introduction

Attention Deficit Hyperactivity Disorder (ADHD) is a neurodevelopmental disorder characterized by persistent inattention and/or hyperactivity-impulsivity. It exerts a significant impact on development and can lead to adverse effects on academic, social, and occupational functioning [1].

Review studies on the prevalence of ADHD in children and adolescents indicate rates ranging from 2% to 7% [2]. In the Spanish population, a prevalence rate of 6.6% has been reported [3]. Furthermore, consistent figures have been observed across different stages of development, with rates of 6.9% in childhood, 6.2% in pre-adolescence, and 6.9% in adolescence [4]. The high prevalence of ADHD, along with its significant impact on the social, academic, and school environments, emphasizes the importance of early diagnosis. Early detection plays a vital role in ensuring that affected individuals receive appropriate support for higher education and improved quality of life standards. However, it should be noted that clinical diagnosis of ADHD can be subjective and variable depending on the diagnostic method employed [4], underscoring the urgent need for more objective and reliable diagnostic tools.

The diagnosis of ADHD reveals an imbalance in the number of males compared to females, with a gender ratio of approximately 3:1 (males vs. females) [5]. Several studies suggest that this disparity arises

* Correspondence to: ETSI Telecomunicación. Universidad de Valladolid, Camino del Cementerio s/n, 47011, Valladolid, Spain.
E-mail addresses: pamacab@lpi.tel.uva.es (P. Amado-Caballero), casaseca@lpi.tel.uva.es (P. Casaseca-de-la-Higuera), salberola56@gmail.com (S. Alberola-López), jm.andres.dellano@gmail.com (J.M. Andrés-de-Llano), villalobos@cop.es (J.A. López-Villalobos), caralb@tel.uva.es (C. Alberola-López).

https://doi.org/10.1016/j.artmed.2023.102630
Received 23 January 2023; Received in revised form 19 July 2023; Accepted 20 July 2023
Available online 4 August 2023

from the difficulty in identifying clear markers in women, potentially leading to underdiagnosis in this population [5,6]. Consequently, there is an urgent need to develop methods that offer a deeper understanding of these gender differences and enable more accurate detection among females. In addition, it is important to acknowledge that ADHD symptoms often attenuate with age, and certain characteristic patterns, such as hyperactivity, may change or fade over time [7]. This poses a challenge in detecting the disorder if it has not been previously diagnosed. Therefore, early diagnosis becomes even more critical in order to identify and address ADHD at the earliest stages.

As we describe in Section 2, various methods have been proposed for automating ADHD diagnosis. Our interest lies in approaches that utilize (physical) activity as input information, given its ubiquitousness, non-invasiveness, and cost-effectiveness. Within this category, we have recently introduced a solution based on deep learning, which exhibits state-of-the-art performance in terms of diagnosis accuracy (figures [8]). In this present paper, our objective is twofold: first, to develop a methodology for identifying patterns in patients activity based on deep neural network activation, and second, to provide physicians with physiologically explainable information regarding both the network and the patients behavior. To this end, the idea of occlusion maps is taken as a starting point; patterns identified with this methodology will be analytically characterized within age and gender subgroups and will let us compare ADHD cases and controls with customary statistical tools. We expect that shedding some light into the network behavior will enable physicians to achieve a better understanding of both the problem and the solution provided in [8]. Furthermore, this approach will provide visual and quantitative information that can be utilized to explain the diagnosis and the patient condition in relation to population values. This will prove valuable in facilitating communication with both the patient and their family, offering a clearer insight into the diagnosis and the patient's overall situation

The remainder of the paper is organized as follows: Section 2 provides an overview of the state-of-the-art in objective diagnosis of ADHD, with a special focus on machine (deep) learning methods and their interpretation. Section 3 presents the materials employed in the study and the proposed methodology for the identification and interpretation of activity patterns associated with ADHD. Results are presented in Section 4 and discussed in Section 5. Finally, Section 6 concludes the paper by summarizing the main conclusions derived from the study.

2. State of the art

2.1. ADHD diagnosis and deep learning

ADHD diagnosis commonly relies on the Diagnostic and Statistical Manual of Mental Disorders (DSM-5) criteria [1].

However, this diagnostic process primarily relies on clinical assessment, which involves questionnaires completed by parents and teachers. The subjectivity inherent in the responses from the patient's environment strongly influences the diagnosis. To address this challenge, various objective diagnostic methods have been proposed over the years to provide more reliable assessments.

One of the main difficulties in finding a reliable diagnostic method for this disorder stems from the existing differences in the expression of symptoms in terms of patient gender or age. This was noticed in [9], where the focus was put on the difficulties in detecting the pathology in girls, since they are more prone to show patterns of inattention over impulsivity or hyperactivity, which is in contrast to the symptom profile commonly observed in boys.

Recent studies have further addressed these complications. Rosch et al. [10] studied the fronto-subcortical functional networks and discovered their alteration in children with ADHD, particularly in girls. Murray et al. [11] identified that females were more prone to exhibit symptoms emerging during early adolescence, whereas males tended to display symptoms starting in childhood. Furthermore, a relationship was found between delayed diagnosis in girls and the manifestation of hyperactivity and impulsivity patterns, which resulted from a later onset of symptoms.

The clinical studies conducted by Mowlem et al. [12,13] have examined these gender differences in depth, where several important findings have been reported. Firstly, they found that the association between hyperactivity/impulsivity, behavioral symptoms, and ADHD diagnosis or treatment status is more pronounced in females compared to males. Consequently, when a girl presents these symptoms, her diagnosis tends to occur earlier than in boys. However, a challenge arises from the fact that external symptoms, such as hyperactivity/impulsivity and conduct problems, are more commonly observed in boys, while girls with ADHD may exhibit lower levels of these symptoms. Furthermore, the skewed gender ratio in many study samples, with a larger representation of boys than girls, complicates the identification of behavioral and emotional patterns in females. The study in [13] revealed the significance of emotional symptoms in girls who meet the diagnostic criteria for ADHD. This finding suggests that emotional symptoms play a crucial role in the female phenotype, providing support for the notion that girls may express their difficulties in distinct ways.

Regarding age, the most relevant change from childhood consists in the attenuation of hyperactive/impulsivity patterns [14] due to the fact that inattention symptoms blend with sleep disorders [15,16] and adolescent depression [17,18]

Despite the abundance of clinical studies that emphasize these differences, to the best of our knowledge, there is a lack of machine learning research that quantitatively measures these differences using objective diagnostic techniques. Existing endeavors in the field primarily focus on the detection of ADHD pathology and the discrimination between individuals with ADHD and healthy subjects.

As for automated diagnosis, traditional machine learning methods are progressively being substituted by deep-learning approaches. From our perspective, we classify them into the two following classes:

- Non-actimetric methods, that comprise both image-based methods (and typically Magnetic Resonance Imaging –MRI–) or physiological signal-based methods (in which electroencephalography –EEG– stands out).
- Actimetric methods, featuring a lower cost and high effectiveness in diagnosis, particularly when combined with deep learning techniques.

Tables 1–3 summarize the most relevant studies that combine deep learning with the information sources mentioned above. The tables are organized in terms of Materials, Methods and Results & Conclusions, as directly reported by their authors.

With regard to MRI studies, the dataset commonly used is *ADHD-200 Global Competition*. Using a CNN as the core of the deep learning system, the highest accuracy is provided by Khullar et al. [21] who combined a 2D-CNN with a LSTM (Long Short-Term Memory), obtaining 98.12%. As for EEG signals, Chen et al. [31] used a CNN to achieve the highest classification accuracy (94,67%) over a group with 50 ADHD and 51 healthy controls. Other network arquitectures such as recurrent convolutional neural networks (RCNN) have been used for classification of ADHD subjects. For instance, Yang et al. [35], obtained 97.36% accuracy with a RCNN fed with EEG data.

Recently, attention mechanisms have gathered interest within the deep learning community. These mechanisms serve as valuable components that can greatly enhance the performance of deep neural networks, particularly when working with sequential data. This is done by enhancing the most relevant parts of the processed data, replicating to some extent cognitive attention patterns. In the last few years, a number of studies have been reported on diagnosis and classification

Table 1
State of the art on DEEP LEARNING approaches for ADHD assessment based on medical-imaging. Results are those reported by the authors.

Medical imaging			
Ref.	Materials:	Methods:	Results and conclusion:
[19]	Resting-state functional MRI images from *ADHD-200 Global Competition* preprocessed using Data Processing Assistant for RestingState fMRI (DPARSF) programs with 197 ADHD (158 male) and 362 (190 male) typically developing children (TDC)	Features extract from *Functional MRI* (fMRI) and *Structural MRI* (sMRI) data with multi-modality 3D-CNN	Accuracy (%) = 69.15
[20]	sMRI from *ADHD-200 Global Competition* with 362 ADHD and 585 TDC	3D fractal dimension complexity map (FDCM) from sMRI with 3D-CNN	Accuracy (%) = 69.01 (for the feature of the gray matter (GM) density
[21]	Some datasets of *ADHD-200 Global Competition*: Kennedy Krieguer Institute (KKI): 61 TDC and 22 ADHD. NeuroIMAGE Sample (NI): 23 TDC and 25 ADHD. New York University Child Study Center (NY): 99 TDC and 123 ADHD. Oregon Health & Science University(OHSU): 42 TDC and 37 ADHD Peking University (PEKING): 146 TDC and 113 ADHD.	Resting state functional magnetic resonance imaging (rs-fMRI) and deep learning-based techniques such as 2-dimensional convolutional neural network (CNN) algorithm and hybrid 2-dimensional convolutional neural network-long short-term memory (2D CNN–LSTM)	Accuracy (%) = 99.50, Sensitivity (%) = 99.40, Specificity (%) = 99.60 (smallest dataset) Accuracy (%) = 97.00, Sensitivity (%) = 96.50, Specificity (%) = 97.40 (bigger dataset) Accuracy (%) = 98.12, Sensitivity (%) = 97.50, Specificity (%) = 98.16 (average of all dataset)
[22]	Resting-state functional MRI images from some datasets of *ADHD-200 Global Competition* : NI: 37 Healthy Control (HC) and 36 ADHD. NY: 110 HC and 147 ADHD and PEKING: 85 HC and 51 ADHD.	Feature extractor from fMRI pre-processed time-series signals with a functional connectivity network, and a classification network.	Accuracy (%) = 73.1 Sensitivity (%) = 65.5, Specificity (%) = 91.6
[23]	Resting-state fMRI and anatomical data from *ADHD-200 Global Competition* with 20 TDC called "controls" and 20 individuals diagnosed with ADHD called ''treatments"	Deep neural network (DNN) using functional connectivity-based fMRI data	Accuracy (%) = 95
[24]	*ADHD-200 Global Competition* with 352 ADHD and 429 HC	Rs-fMRI data using 15 important region of interest(ROIs) for training three different models to classify ADHD: Separate Channel CNN–RNN with Attention (ASCRNN), Separate Channel dilate CNN–RNN with Attention (ASDRNN) and Separate Channel CNN - slicing RNN with Attention (ASSRNN)	Accuracy for ASSRNN model(%) = 70.6
[25]	*ADHD-200 Global Competition* with 286 ADHD and 340 TDC in the training set and 73 ADHD and 89 TDC in the test set.	4-D CNN arquitecture with spatio-temporal deep learning models & rs-fMRI for automatic ADHD diagnostic	Accuracy (%) = 71.3 AUC = 0.80
[26]	fMRI from *ADHD-200 Global Competition*	Deep Channel Self-Attention Factorization for classificate ADHD	Precision (%) = 99.87 Recall (%) = 99.90 F1-Score (%) = 99.88 Accuracy (%) = 99.0
[27]	Resting-state fMRI data from *ADHD-200 Global Competition,* specifically the datasets from New York University medical center, Kennedy Krieger Institute, and Peking University	Auto-encoding network with attention mechanism	Accuracy (%) = 98.9
[28]	fMRI from *ADHD-200 Global Competition* over 281 children with ADHD and 266 normal control children	Attention mechanism with auto-encoder for ADHD classification	Accuracy (%) = 77.2
[29]	fMRI from *ADHD-200 Global Competition* over 422 ADHD and 597 HC	Separated Channel Attention Convolutional Neural Network	Accuracy (%) = 68.6
[30]	fMRI from *ADHD-200 Global Competition*	Spatiotemporal attention auto-encoder (STAAE) with rs-fMRI for classification of ADHD patients	Accuracy (%) = 72.5

of ADHD, using functional MRI (fMRI) data. Notably, the approaches in [28,29] achieved classification accuracy figures above 90% over a database where other deep learning techniques struggled to reach 80%. Bakhtyari et al. [38] used a deep neural network combining convolutional LSTM layers together with attention mechanisms over EEG data. They obtained 99.75% accuracy in diagnosing ADHD.

The use of deep learning over actimetry has also provided interesting results. Muñoz et al. [39] obtained 93.7% accuracy in a group with 11 ADHD and 11 healthy controls with an ankle accelerometer and a CNN architecture. More recently, we proposed [8] an ensemble architecture that used a CNN to classify activity patterns that were further combined for final diagnosis using a Support Vector Machine (SVM). Data was obtained using an actimeter placed on the dominant wrist. The diagnostic accuracy was 98.6%.

2.2. Interpretation of deep learning

CNNs are widely used to solve classification problems, especially in the field of disease detection. However, they find a major difficulty in explaining the underlying issues motivating the disease, since they act as black boxes and do not provide a simple association between the results obtained and their clinical explanation. Nevertheless, different methodologies have been developed to address this issue. The most widespread are:

- *DeepDream* is an algorithm created by Google; it provides means for visualizing the patterns learned by a neural network by sending an image through the network, calculating the gradient of the image with respect to the activations of a particular layer and returning an image that would represent the maximum activation of the network for the classes under analysis [42].

Table 2
State of the art on DEEP LEARNING approaches for ADHD assessment based on biomedical signals. Results are those reported by the authors.

Biomedical signals			
Ref.	Materials:	Methods:	Results and conclusion:
[31]	EEG data from 50 children with ADHD (9 girls, mean age: 10.44 ± 0.75) and 51 handedness- and age-matched controls.	CNN arquitecture	Accuracy (%) = 94.67
[32]	EEG data from 13 ADHD-C [9 boys, 4 girls; age: 8.5 ± 0.7 y (mean ± standard error)], 12 ADHD-I [7 boys, 5 girls; age: 8.75 ± 0.65 y] and 14 controls [8 boys, 6 girls; mean age: 8.92 ± 1.38 y].	CNN arquitecture	Accuracy (%) = 99.46, Recall (%) = 99.45, Precision (%) = 99.48 and Kappa = 0.99
[33]	EEG data from 144 participants. 52 participants (10 female, age:10.9 ± 2.4; IQ: 100 ± 12) fulfilled criteria for ADD(ADHD inattentive) according to ICD-10 (F98.8), 48 were diagnosed with the combined subtype (ADHD; ICD-10 F90.0 or F90.1) (12 female, age: 10.6 ± 1.9; IQ: 103 ± 13). and the remaining 44 participants were healthy control children (15 female,age: 11.3 ± 2.2; IQ: 103 ± 12)	CNN arquitecture	Accuracy (%) = 83
[34]	EEG data from 50 children with ADHD (nine girls, mean age: 10.44 ± 0.75) and 57 controls who were matched for age	CNN arquitecture	Accuracy (%) = 90.29
[35]	Motor imagery dataset*EEGMMIDB*, from PhysioNet (subjects in the study: 108)	Recurrent convolutional neural network (RCNN)	Accuracy (using all channels) (%) = 97.36 Accuracy (using a selection of channels) (%) = 92.31
[36]	EEG signals recorded from 31 ADHD children and 30 healthy children	Deep CNN	Accuracy (%) = 98.48
[37]	EEG data from a total of 40 participants including 20 healthy adults (10 males, 10 females) and 20 ADHD adult patients (10 males, 10 females) group.	Four layer CNN	Accuracy (%) = 88 ± 1.12, AUC (%) = 96 ± 0.74
[38]	EEG data from 46 children with ADHD and 45 children in the control group, in the age range of 7–12 years	ConvLSTM with attention mechanism with 5 fold cross validation.	Accuracy (%) = 99.75

Table 3
State of the art on ADHD assessment through activity measurement. Results are those reported by the authors.

Activity performing a specific task			
Ref.	Materials:	Methods:	Results and conclusion:
[39]	22 patients, 11 ADHD and 11 healthy subjects	Two accelerometers on the wrist and ankle respectively to analyze data obtained in 6 school hours and a CNN Arquitecture	Accuracy = 0.8570 , Sensitivity = 0.6 and Specificity = 1 for the wrist and Accuracy= 0.937, Sensitivity =0.8 y Specificity=1 for the ankle. No specifics on the differences between ADHD and controls activity patterns were provided.
[40]	19 ADHD patients and 24 healthy controls aged 6–11 years old.	Activity signals obtained through two inertial movement sensors placed on waist and the non-dominant ankle during the visit to the psychiatrist (1 h approximately).	Best results are achieved for a SVM-based classifier with 10 features; accuracy = 95.12%, sensitivity = 94.44% and specificity = 96.65%.
[8]	73 ADHD (combined kind) patients and 75 healthy controls between the ages of 6 and 15 years old.	Actigraphy device placed on their dominant wrist & CNN Arquitecture + SVM.	Accuracy (%) = 98.6 & Sensitivity (%) = 97.62 & Specificity (%) = 99.52
[41]	51 ADHD patients and 52 with other disorders termed as clinical controls between the ages of 17 and 67 years old.	Wrist-worn actigraph device for movement activity and a compact battery-powered chest-worn device for ECG-based heart rate data. + SVM.	Accuracy (%) = 98.43 & F-Measure = 98.42 & Sensitivity (%) = 98.33 & AUC = 0.983

- *Class activation maps (CAM)*, proposed by Zhou et al. [43], highlight those regions of the image used by the CNN to distinguish between the different categories, using global average pooling (GAP).
- *Grad-CAM*, designed by Selvaraju et al. [44], consists of a generalization of CAM that employs the average clustering of the class probability gradients.
- *Occlusion Maps.* This technique was first implemented by Zeiler et al. [45] in order to understand CNNs and has been since used in multiple occasions to gain insight into the behavior of neural networks. It works by defining a mask, either of fixed or variable size, which will be placed on the input image and will consequently hide some image information to the CNN. The class probability provided by the CNN fed by this distorted input will be a en estimate of the importance of the hidden area for the classification (higher probability means less importance). The mask is then slided, the process is repeated and the output values are stored in a matrix, which is then resized to have the same dimensions as the original image.
- *Attention mechanisms* have demonstrated their utility not only for improving performance but also for facilitating interpretation within deep learning models. By highlighting the most relevant components of input signals or intermediate features, attention mechanisms provide valuable insights into the underlying data.

We are aware of some studies that have applied some of these techniques to understand ADHD. Dubreuil-Vall et al. [37] applied DeepDream to find out what type of inputs optimally excite the output nodes of a network trained with EEG signals from adults diagnosed with ADHD. Chen et al. [34] used EEG signals to train a 3D-CNN and further used Grad-CAM to derive the class-discriminative region in the spatial-frequency space for the 'ADHD' or 'control' categories. Dong et al. [28] employed attention mechanisms to interpret functional connectivity patterns in ADHD patients. Specifically, these mechanisms were employed to extract factor matrices that encapsulated maximal information, enabling the identification of connected regions of interest within fMRI frames.

To the best of our knowledge, no studies to date have reported the utilization of interpretation maps within the field of actimetry. Additionally, the application of deep learning algorithms with interpretation maps has primarily focused on qualitative analysis of the obtained

results. However, our proposal aims to push the boundaries further by employing Gaussian mixture models to quantitatively assess these results.

According to this review, our proposal is built upon the following key concepts:

- There is sufficient evidence to support the significant influence of age and gender on ADHD diagnosis. Despite this, current automated diagnosis methods do not effectively incorporate this information.
- As previously stated, the application of deep learning interpretability techniques in the field of ADHD with actimetry remains unexplored

Our proposal contributes to the field by providing some insight into these two topics.

3. Materials and methods

3.1. Materials

Our group of subjects consists of 139 children, aged between 6 and 15. 70 of them have been diagnosed with combined ADHD according to DSM-V while the remaining 69 are healthy. None of these subjects were on medication at the time of data collection. Hereinafter, individuals in the first group will be referred to as *cases* and those in the second group as *controls*.

The procedure to diagnose ADHD was the following:

Parents and educators were involved in completing the ADHD RS-IV questionnaire [Attention Deficit Hyperactivity Disorder Rating Scale - IV] [46]. This questionnaire has been proven reliable and valid, and matches the diagnostic criteria outlined in the DSM-V. Furthermore, its utility extends to the classification of different subtypes of ADHD. All ADHD cases exceeding the psychometric criteria in the RS-IV questionnaire completed a clinical interview also matching the DSM-V. This clinical interview ensures the existence of a persistent pattern of symptoms, their presence in two or more settings before the age of twelve, and clinically significant impairment in social or academic activity. In summary, the case is defined by the joint presence of psychometric and clinical criteria. Controls were assessed using the same procedure, excluding the presence of ADHD using the ADHD RS-IV.

We further subdivided each group according to two criteria, namely, age and gender:

- Age subgroups: the primary subgroup consists of subjects aged 6 to 11, representing those attending primary school. On the other hand, the secondary subgroup includes subjects aged 12 to 15, corresponding to the junior high school age range.
- Gender subgroups: males and females.

The final group and subgroup distribution is summarized in Table 4.We created additional subgroups by combining the intersection of the two criteria above, i.e., "primary males" (PM), "primary females" (PF), "secondary males" (SM) and "secondary females" (SF). Age and gender subgroups will be collectively referred to as *main subgroups*. Ages for each subgroup were distributed as follows (mean ± standard deviation): 7.9 ± 1.7 (PM), 13.1 ± 1.1 (SM), 7.2 ± 1.0 (PF) and 12 ± 1.7 (SF).

Actimetry recordings were acquired with an ActiGraph GT3x device placed in the non-dominant wrist. All subjects were monitored in their regular daily activity for approximately 24 h. As input data, we utilized the magnitude signal derived from acceleration measurements in all three Cartesian axes, employing a sampling rate of 1 Hz.

This study was approved by the "Área de Salud de Palencia" Research Ethics Committee (Register number: 2022/009). Subjects provided their informed consent before the recordings.

Table 4
Groups and subgroups of the study.

Cases	Males	Females	Total
Primary	47	12	59
Secondary	9	2	11
Total	56	14	70
Controls	Males	Females	Total
Primary	50	11	61
Secondary	6	2	8
Total	56	13	69

3.2. Methods

The methodology employed for diagnosing subjects in each subgroup, investigating the impact of age and gender on the detection of ADHD, follows a similar approach as presented in our previous work [8]. This methodology can be broadly summarized into two distinct steps:

1. Data preprocessing: Actigraphy signals were transformed into spectrograms so that a time–frequency representation of the signal was obtained. The following process was carried out:
   - First, two records were created to differentiate between nocturnal and diurnal activity (using data time stamps).
   - The signals were fragmented into 1800-, 300- and 60-second intervals, corresponding to long, medium and short term activities.
   - Finally, time consecutive spectrograms were created out of these intervals. These spectrograms are stored as column vectors, and horizontally concatenated to build a 2D time–frequency image representation of the original signal. Each of these images will be hereinafter referred to as *window*.
2. The obtained windows constitute the input to the CNN, so each of them is classified as an ADHD or non-ADHD pattern. Subsequently, an SVM classifier is utilized for patient diagnosis, where the input to the classifier is the proportion of windows identified as ADHD by the CNN. The network presented (see Fig. 1) consists of 3 convolutional layers with 32, 64 and 128 filters respectively, followed by an activation layer (ReLU) and a normalization layer (BatchNormalization), a fully connected layer and a softmax layer. The architecture of the CNN has been validated in [8].
   This process is carried out both for nocturnal and for diurnal activity. Although we addressed in [8] the three types of signal fragmentation mentioned above, for the sake of simplicity, this paper will focus on 1800-second intervals as they demonstrated superior diagnostic accuracy.
   In order to analyze age and gender differences, we have trained eight networks, namely, {male,female,primary,secondary}, for both diurnal and nocturnal activity periods. The training/testing procedure has been carried out by means of 10-fold cross-validation. The procedure is shown in Fig. 2. The upper branch of the figure shows the customary procedure for window classification into case/control categories. In this paper, we emphasize the significance of the lower branch as it provides a mechanism to explore the distinctions between cases and controls by delving into the internal functioning of the CNN. Specifically, for each fold we obtain the occlusion maps on the test set using only the windows for which the softmax provides a decision probability above 90%. The specific procedure has three stages (see Fig. 3), which are now described in detail:

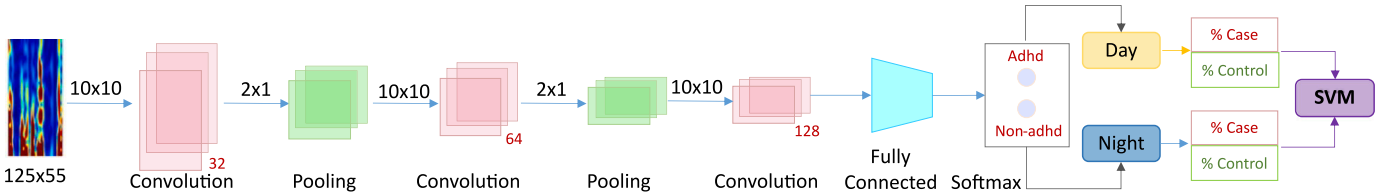

Fig. 1. Structure of the network and the training process of the diagnosis system designed in [8].

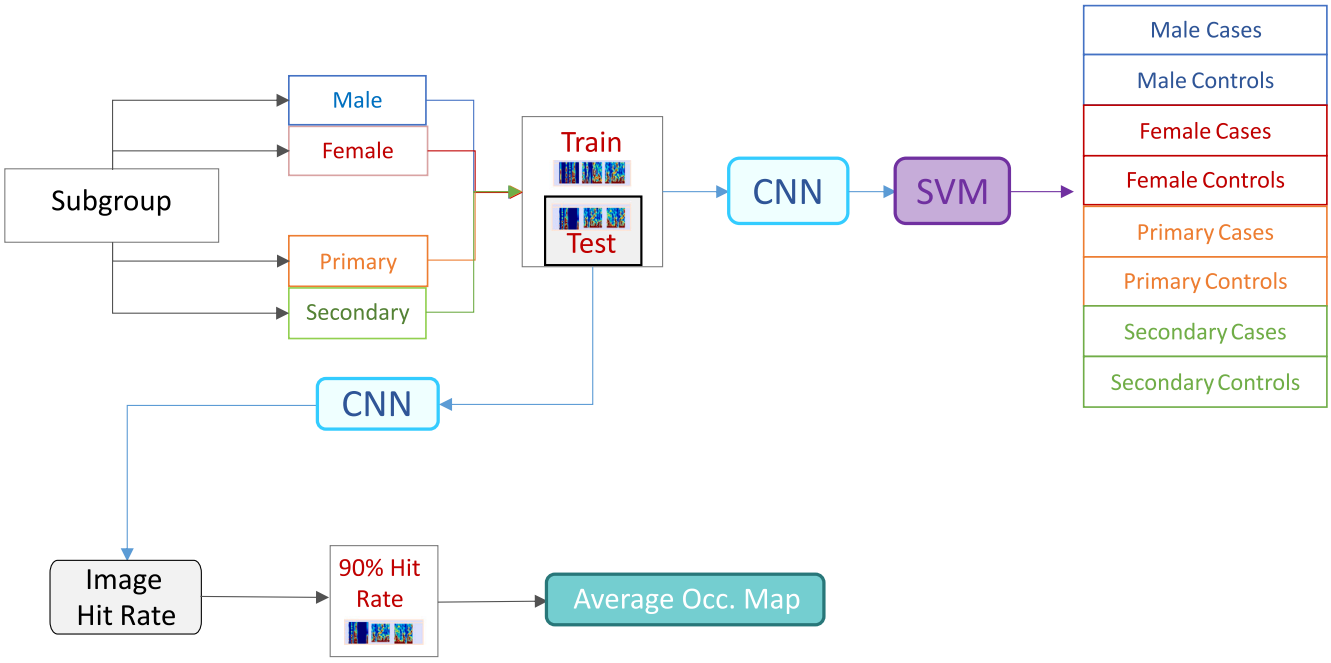

Fig. 2. Overview of the classification (upper branch) and occlusion map determination (lower branch). The color code in the upper branch indicates the classification in Cases/Controls for each subgroup for which a CNN is trained (either for nocturnal or for diurnal activity).

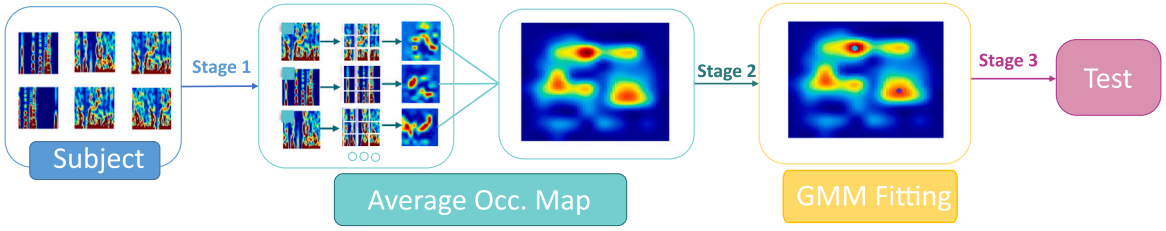

Fig. 3. Procedure for the interpretation method. Occlusion maps are obtained out of inputs of the CNN for which decision confidence is higher than 90%. The block labeled as "GMM fitting" carries out the operation described in Eq. (1). The block labeled as "Test" executes the hypothesis tests on the samples indicated in Eqs. (3) and (4).

3.2.1. Occlusion maps

For every window that meets the aforementioned selection criterion, we have computed its occlusion map. Maps obtained from different selected windows of the same subject undergo normalization to their maximum values and are subsequently pixel-wise averaged, resulting in a singular occlusion map per subject. Given that separate studies were conducted for age, gender, and diurnal/nocturnal activity, each patient will have four distinct occlusion maps representing each study. Population-level maps for each group are derived by computing the median map across all patients within the respective group.

3.2.2. Gaussian mixture model fitting

We have fitted a Gaussian mixture model (GMM) to each occlusion map. Specifically, denoting by $m(x, y)$ the occlusion map at point (x, y) pertaining to some specific domain $\chi \subset \mathbb{Z}^2$ within the 2D grid, and $f(x, y; \boldsymbol{\theta}_i)$ a 2D Gaussian density function with parameters $\boldsymbol{\theta}_i$, the fit is obtained by

$$\min_{p_1,p_2,\boldsymbol{\theta}_1,\boldsymbol{\theta}_2} \sum_{(x,y)\in\chi} \left(m(x,y) - \sum_{i=1}^{2} p_i f(x,y;\boldsymbol{\theta}_i) \right)^2 \tag{1}$$

with

$$\boldsymbol{\theta}_i = \left[\begin{array}{ccccc} \eta_{x_i} & \sigma_{x_i} & \eta_{y_i} & \sigma_{y_i} & \rho_{x_i y_i} \end{array} \right], \tag{2}$$

i.e., the parameter vectors include means (denoted by letter η) and standard deviations (denoted by letter σ) as well as the Pearson correlation coefficient (ρ) between the two components. Subindices indicate the direction along which each parameter is calculated (specifically, –x– the horizontal axis and –y– the vertical axes). Hereinafter $[\boldsymbol{\theta}_i]_k$ will denote the kth component of this vector, $(1 \le k \le 5)$.

3.2.3. Statistical analysis of the fitted parameters

The objective is to assess the presence of statistically significant differences in the GMM fits between ADHD subjects and controls within each subgroup. For this purpose, the following procedure has been carried out:

- First, we looked for the dominant Gaussian distribution in each of the subjects, i.e., the density function associated with the largest p_i in Eq. (1). Let $\theta^{ca}_{d,j}$ denote the parameter vector of the dominant distribution corresponding to subject j in the group of cases ($1 \leq j \leq M$) belonging to some subgroup. Correspondingly, $\theta^{co}_{d,j}$ denotes the dominant parameter vector of the jth control ($1 \leq j \leq N$). In addition, we define

$$\theta^{ca}_{d}[k] = \left[\begin{array}{ccc} \left[\theta^{ca}_{d,1}\right]_k & \cdots & \left[\theta^{ca}_{d,M}\right]_k \end{array} \right] \tag{3}$$

$$\theta^{co}_{d}[k] = \left[\begin{array}{ccc} \left[\theta^{co}_{d,j}\right]_k & \cdots & \left[\theta^{co}_{d,N}\right]_k \end{array} \right] \tag{4}$$

  i.e., the vectors consisting respectively of M and N entries that correspond to the kth component of the dominant vector defined in (2) for both cases and controls. These vectors will be hereinafter referred to as *the samples*.
- The samples will be compared to find statistical differences between them. Specifically, a Gaussianity test will be first carried out on each sample; if Gaussianity applies in both, an unpaired t-test is used. Otherwise, a Mann Whitney U-test is employed.
- The appropriate test is executed for all the parameters in Eq. (2). Whenever significant differences are found (i.e., the p-value is lower than 0.05) boxplots are displayed.

For completeness, we also analyzed the Cauchy–Schwarz divergence [47] between the fitted distributions. Specifically, letting

$$\boldsymbol{\Theta} = \left[\begin{array}{cccc} \theta_1 & p_1 & \theta_2 & p_2 \end{array} \right] \tag{5}$$

where subscript 1 denotes the dominant Gaussian, and denoting $g^X_j(x, y; \boldsymbol{\Theta})$, $X = \{ca, co\}$ the fitted distribution for the jth subject for that group, the divergence between the ith case and jth subject belonging to group X is defined as

$$d^{ca,X}_{i,j} = d\left(g^{ca}_i(x, y; \boldsymbol{\Theta}), g^X_j(x, y; \boldsymbol{\Theta})\right), \tag{6}$$

with $1 \leq i, j \leq M$, $i \neq j$ for $X = ca$ and $1 \leq i \leq M$, $1 \leq j \leq N$, for $X = co$. Eq. (6) is extended accordingly to age and gender subgroups.

4. Results

This section focuses on the statistical analysis of occlusion maps in the defined subgroups. Distribution distances, mixture parameter distributions, and representative occlusion maps have been thoroughly examined and the main results are presented. These representations offer physicians objective visual and quantitative tools that can be utilized in their practice to elucidate the results obtained from the decision support tool described in [8]. The depicted occlusion maps will represent population-level maps.

To examine differences related to the age and gender of the patients, we analyzed the outcomes of the networks mentioned in Section 3. Additionally, we assessed the performance of these networks on various intersection subgroups. We first calculated the Cauchy–Schwarz divergence between distribution fits for the primary subgroup. Fig. 4 shows the results for nocturnal activity. As can be inferred, distances between each pair of cases tend to be smaller than case-control distances. A similar behavior can be observed for the secondary subgroup and diurnal activity (see Fig. 5). These results motivate further analysis on quantitative differences between cases and controls in different subgroups.

Tables 5 and 6 show the p-values obtained from pairwise-comparing each of the five components in Eq. (2) (plus the weighting term of the dominant Gaussian) for cases and controls in each of the indicated subgroups. The Primary/Secondary CNNs have been used to obtain the results in Table 5, while for Table 6 networks are Male/Female. Results are provided for each subgroup as well as for diurnal and nocturnal activity. Results indicate that both η_y and σ_y, i.e., those parameters directly related to information in the frequency domain, take the lead in terms of statistical significance. Hereinafter, we will concentrate on these two parameters.

Table 5
P-values from the hypothesis tests for the age training. CNNs used are Primary/Secondary both for nocturnal and diurnal activities. p is the weighting factor of the dominant Gaussian; the other five columns refer to the parameters defined in Eq. (2).

	p	η_x	η_y	σ_x	σ_y	ρ_{xy}
SECONDARY						
NIGHT	0.5593	0.975	0.4853	0.1881	0.9361	0.2201
DAY	**0.0029**	0.6263	**0.0097**	0.1563	0.1296	0.1672
PRIMARY						
NIGHT	0.7251	**0.0107**	**0.0**	0.5461	0.5531	0.7409
DAY	0.2418	0.1228	0.3864	0.1459	0.9548	0.5923
PRIMARY FEMALES						
NIGHT	0.8086	0.1855	**0.0008**	0.9261	0.116	0.29
DAY	0.7804	0.3523	0.2941	0.1679	0.1499	0.7531
SECONDARY FEMALES						
NIGHT	0.7321	0.4578	0.8193	0.7435	0.5156	0.1201
DAY	0.5138	0.975	**0.0008**	0.3523	0.8430	0.766
PRIMARY MALES						
NIGHT	0.3388	0.4279	**0.0282**	**0.0228**	**0.0366**	**0.0001**
DAY	0.3352	**0.0181**	0.5808	0.4381	**0.0052**	0.9728
SECONDARY MALES						
NIGHT	0.499	0.436	0.2308	0.6077	0.5374	0.703
DAY	**0.0453**	0.3623	0.797	**0.0009**	**0.0124**	0.5292

Table 6
p-values from the hypothesis tests for the gender training. CNNs used are Male/Female both for nocturnal and diurnal activities. p is the weighting factor of the dominant Gaussian; the other five columns refer to the parameters defined in Eq. (2).

	p	η_x	η_y	σ_x	σ_y	ρ_{xy}
MALES						
NIGHT	**0.0256**	**0.0302**	0.8092	0.8729	0.9884	0.3875
DAY	0.6188	0.547	0.4905	0.0582	0.2272	0.4203
FEMALES						
NIGHT	0.1365	0.2141	0.9744	**0.0489**	**0.048**	0.8385
DAY	0.6361	0.6468	0.0660	0.8180	0.7614	0.2365
PRIMARY FEMALES						
NIGHT	0.8086	0.2887	0.2967	0.3375	0.3585	0.0781
DAY	0.7804	0.5368	0.3753	0.9772	0.8938	0.3109
SECONDARY FEMALES						
NIGHT	0.7321	0.8417	0.8343	0.5258	0.6943	0.0629
DAY	0.5138	0.7119	**0.0247**	0.0986	0.5557	0.3151
PRIMARY MALES						
NIGHT	0.3388	0.4494	0.1312	0.9453	0.247	**0.0089**
DAY	0.3352	0.2294	0.1067	0.125	0.854	**0.0195**
SECONDARY MALES						
NIGHT	0.499	0.2138	0.4494	0.0576	0.06604	0.5556
DAY	**0.0453**	0.4861	0.3205	**0.0005**	**0.0424**	0.6336

4.1. Insight on η_y

Regarding η_y, we present the boxplots obtained for the most relevant subgroups. In particular, Fig. 6 shows boxplots for ADHD cases (left box) and controls (right box) in Primary (left), PM (center) and PF (right) subgroups for nocturnal activity and Fig. 7 shows representative

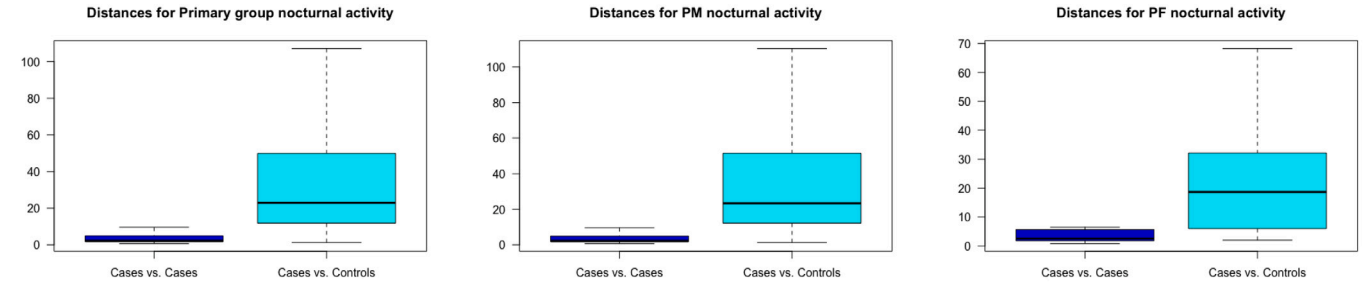

Fig. 4. Cauchy–Schwarz divergence between cases (left) and cases and controls (right) for nocturnal activity period. The CNN used is primary-nocturnal. PM: primary male. PF: primary female.

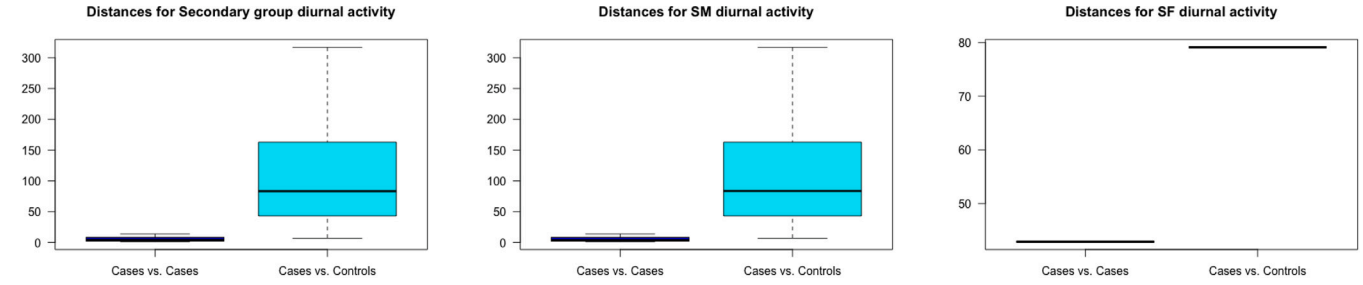

Fig. 5. Cauchy–Schwarz divergence between cases (left) and cases and controls (right) for day activity period. The CNN used is secondary-diurnal. SM: secondary male. SF: secondary female.

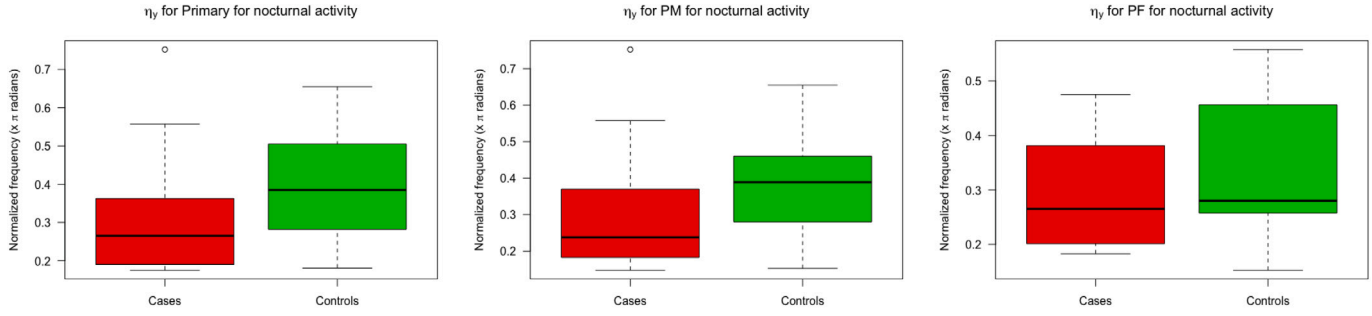

Fig. 6. Boxplots for η_y for Primary controls (right) and Primary Cases (left) for the primary-nocturnal CNN.

occlusion maps from subjects in these subgroups, with upper row for cases and lower row for controls.

Relative to the secondary networks, Fig. 8 shows boxplots for cases (left box) and controls (right box) in Secondary (left) and SF (right) subgroups for diurnal activity. The representative occlusion maps from subjects in these subgroups can be seen in Fig. 9; specifically, the two upper figures correspond to ADHD cases and the lower images to controls (left Secondary, right SF). The CNN used in this case is secondary-diurnal.

4.2. Insight on σ_y

With respect to σ_y, the most significant results were obtained on the primary and secondary male subgroups. More specifically, Fig. 10 shows boxplots for ADHD cases (left box) and controls (right box) in the PM subgroup for diurnal and nocturnal activity (left and center, obtained from primary-diurnal and primary-nocturnal CNNs respectively) and for SM nocturnal activity (right, with secondary nocturnal CNN). The occlusion maps for some subjects from these subgroups are shown in Figs. 11 and 12; specifically, Fig. 11 refers to PM diurnal activity while Fig. 12 refers to SM nocturnal activity (cases left, controls right).

4.3. Occlusion vs. attention maps

Given the usefulness of attention mechanisms in interpreting the behavior of neural networks to understand brain connectivity in ADHD patients [28], we have conducted experiments to explore their applicability to our problem. To achieve this, we have employed a method based on spatial attention, as outlined in [48]. This approach involves extracting attention weights using spatial patches over the feature maps. Firstly, we apply average pooling and max pooling operations to each channel of the feature map. The results of both pooling operations are then concatenated to form a single descriptor. Subsequently, we utilize a convolutional layer and a sigmoid function to generate the desired attention map from the concatenated feature descriptor.

Figs. 13 and 14 show comparative examples of attention and occlusion maps for male and primary subjects respectively. In both figures, the occlusion maps (right) show the most meaningful regions highlighted, whereas the attention maps (left) show the same for the feature channel extracted from the third convolutional layer. The figures clearly demonstrate that the highlighted regions in the occlusion maps exhibit a higher degree of regularity, allowing for straightforward quantification using a simple model like the proposed Gaussian mixture. Furthermore, the information provided by the occlusion maps can be easily explained in the time–frequency domain since it is directly

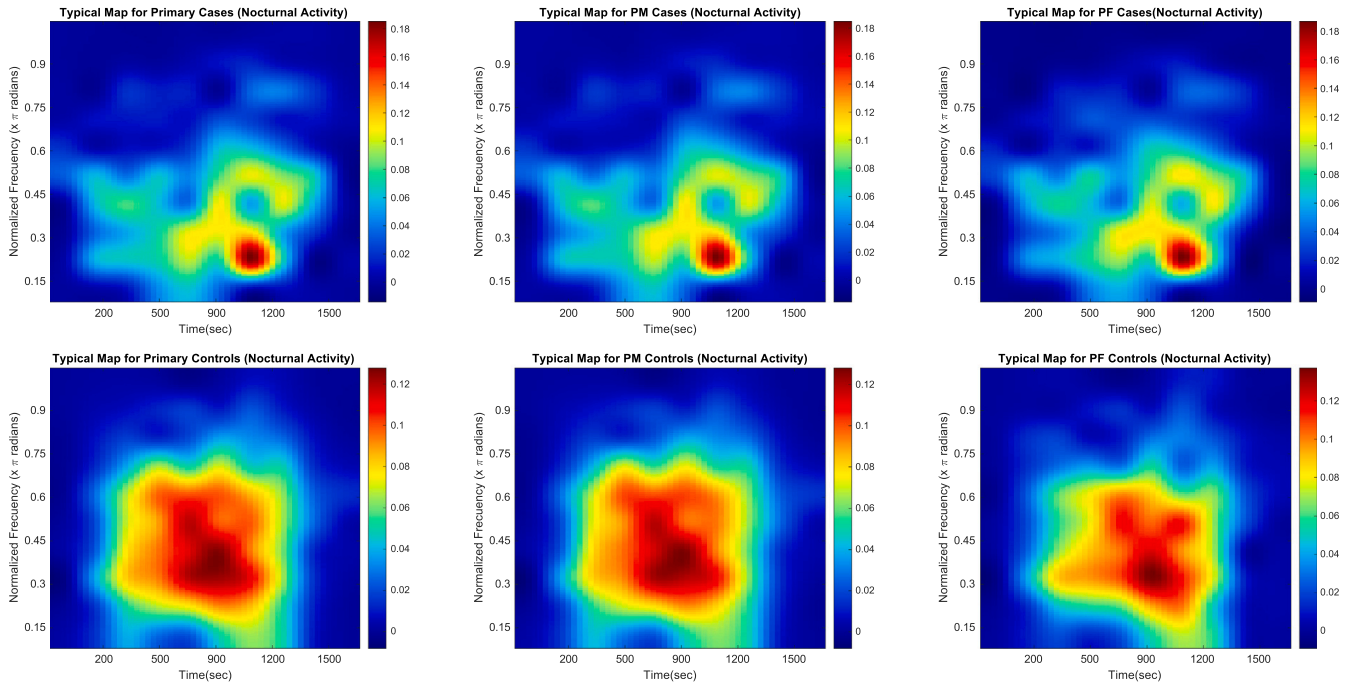

Fig. 7. Occlusion Maps obtained for the Primary cases (upper) and Primary controls (lower), for the primary-nocturnal CNN. Center and rightmost images are PM and PF, while leftmost images integrate both genders.

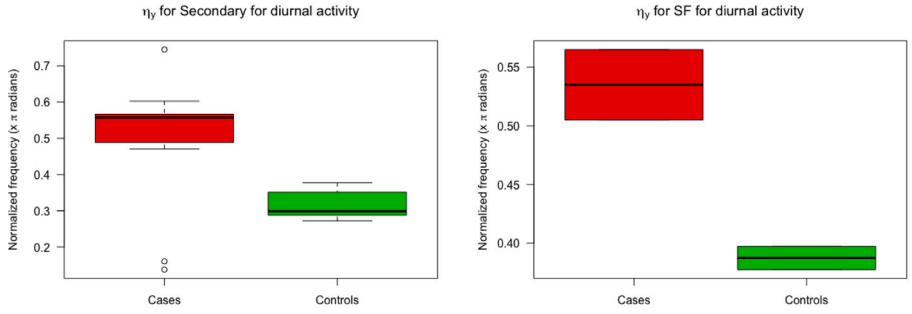

Fig. 8. Boxplots for η_y for Secondary controls (right) and Secondary Cases (left) for the secondary-diurnal CNN.

derived from the input spectrogram. Conversely, the energy regions in the attention maps appear more scattered and less regular. While they may contain relevant information regarding the location and shape of meaningful structures in the time–frequency domain, they turn out not to be as amenable to modeling for the extraction of quantitative information.

5. Discussion

The findings presented in Section 4 suggest the existence of distinctive features in the differences between cases and controls, according to the patient's age and gender. Divergence measures between cases and controls presented in Figs. 4 and 5 show this separation, which is consistent with the system's ability to perform classification. Based on this hypothesis, quantification of occlusion maps seems a good starting point to understand the specific behavior of each subgroup.

Regarding the results obtained from the GMM fit to the occlusion maps (Eq. (1)), the frequency behavior is more relevant to understand differences between cases and controls, as observed in Table 5, where η_y and σ_y are shown to be the most significant parameters. Focusing on the primary and secondary subgroups, Figs. 6, 8 and 10 show that day and night have a different influence when it comes to differentiating between cases and controls, which is coherent with clinical evidence. [14,16] report that adolescents with ADHD often experience sleep difficulties, which subsequently impact the proper development of their daily activities [49]. Although these differences in sleep disorders are present in both nocturnal and diurnal activity, they are more relevant in the occlusion maps of the latter, as we detail below.

Parameter η_y is consistently lower for ADHD cases than that of controls in the primary subgroup as well as in PM and PF (see Fig. 6). It is worth noting that this effect is less prominent in the PF subgroup, which aligns with the challenges observed in diagnosing females with ADHD, [9–13]. This discrepancy may be attributed to the fact that inattention is the prevailing pattern within the PF subgroup. The maps in Fig. 7 highlight that nocturnal activity in ADHD cases exhibits smaller high-valued areas compared to controls, although these differences are accompanied by notable temporal variations. In contrast, the activity of controls tends to be more temporally concentrated, with larger high-valued areas that reach their maxima near the center of the occlusion map.

Regarding the secondary subgroup, η_y proves to be more discriminative during diurnal activity. Fig. 8 illustrates that this parameter is significantly higher in ADHD cases compared to controls, indicating a greater energy influence in the network outcome at high frequencies. This can be interpreted as heightened variability in the movement

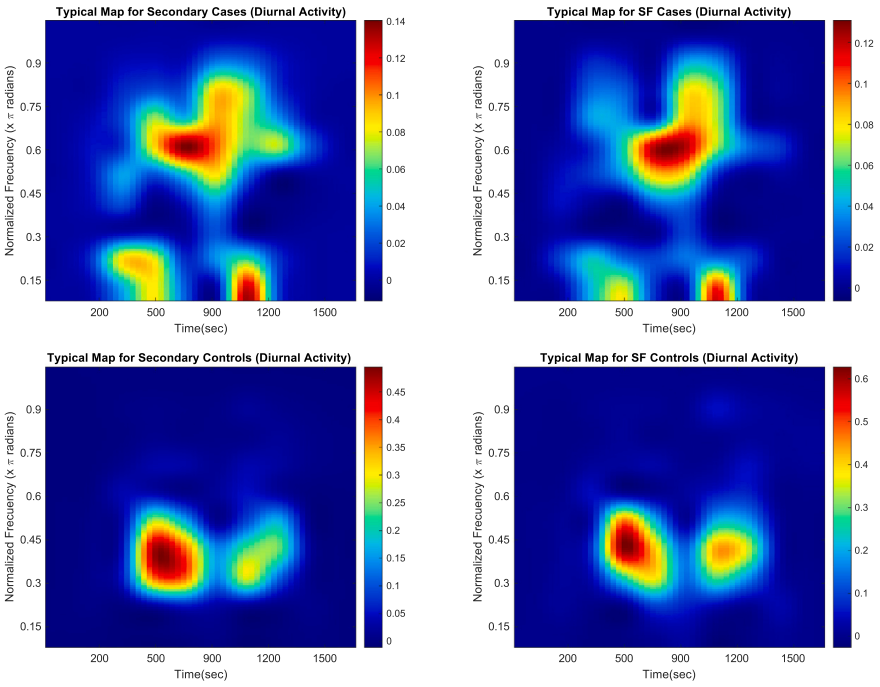

Fig. 9. Occlusion maps obtained for the secondary cases (upper) and secondary controls (lower), for the secondary-diurnal CNN.

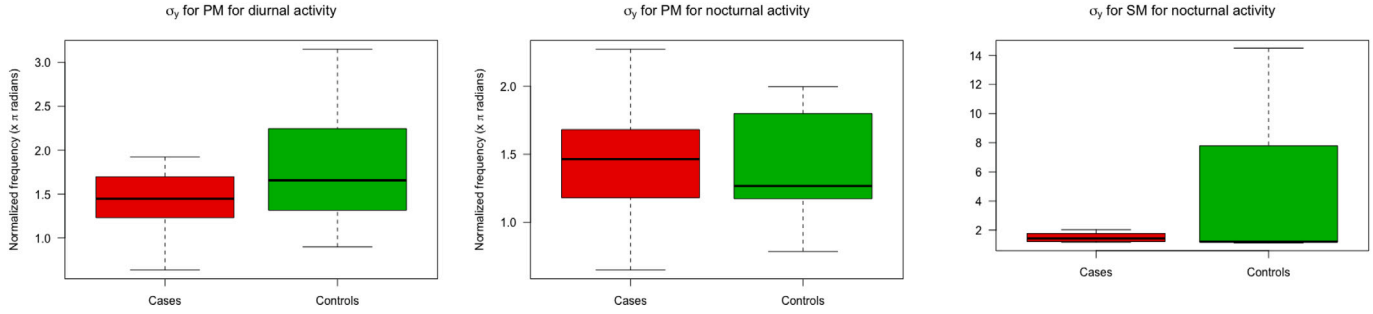

Fig. 10. Boxplots for σ_y for controls (right) and Cases (left) of Primary and Secondary males. CNN used: leftmost figure primary-diurnal, center: primary nocturnal, rightmost: secondary-nocturnal.

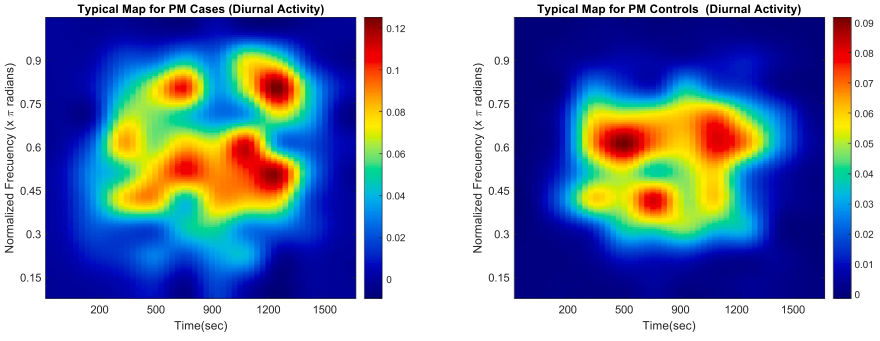

Fig. 11. Occlusion Maps obtained for the Primary Male controls (right) and Primary Male cases (left) for the primary-diurnal CNN.

pattern of individuals with ADHD throughout the day. In the occlusion maps displayed in Fig. 9, ADHD cases exhibit the highest activity concentration at frequencies around 0.6π radians, whereas controls show concentrated activity within the range of 0.3π to 0.45π radians. Furthermore, the controls' pattern exhibits a distinct bimodality in the central region of the temporal dimension, characterized by highly condensed activity in that area. In contrast, ADHD cases display an extended zone where activity spreads out across the entire window, indicating a different distribution pattern.

Results concerning σ_y are particularly interesting for males in age groups. When observing the maps depicted in Fig. 11, a notable distinction arises in the primary subgroup. In diurnal activity, the maximum of the distribution for ADHD cases is closer to the end of the activity compared to controls. Additionally, cases in the PM subgroup exhibit

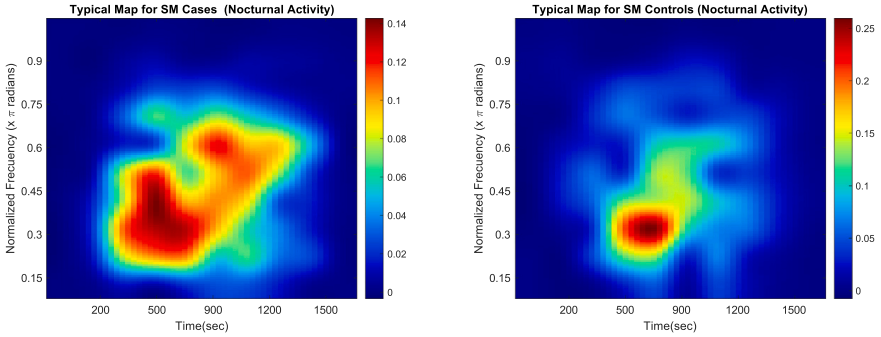

Fig. 12. Occlusion Maps obtained for the Secondary Male controls (right) and Secondary Male cases (left) for the secondary-nocturnal CNN.

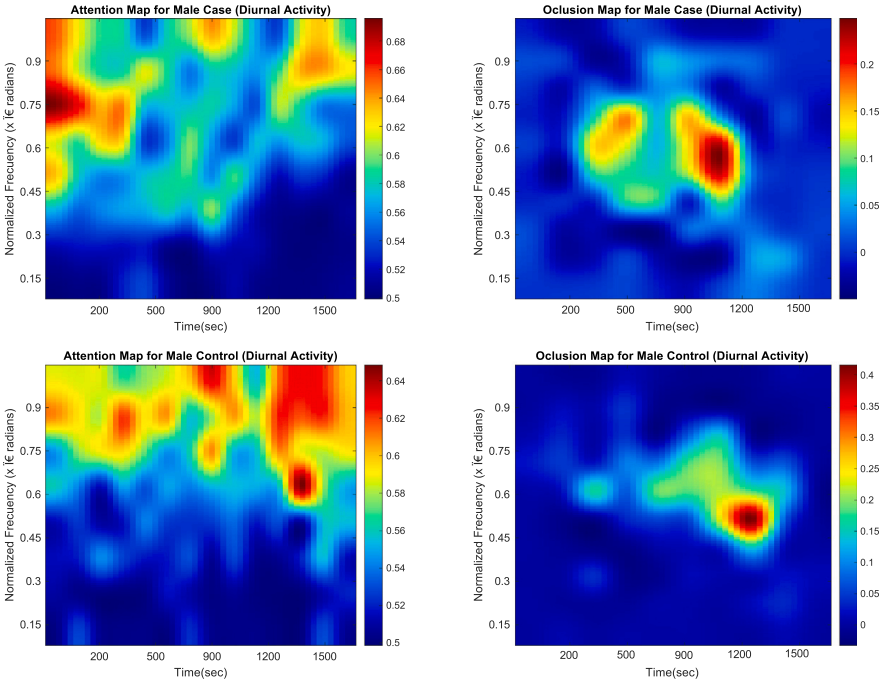

Fig. 13. Maps obtained for the Male cases (upper) and Male controls (lower), for the male-diurnal CNN. Center and rightmost images are the maps, while leftmost images represent the input of the network.

higher frequencies during this period of the day. Conversely, both PM and SM subgroups demonstrate a wider range of frequencies in ADHD cases compared to controls during nocturnal activity, as illustrated in Fig. 10. This characteristic is also evident in the SM occlusion maps depicted in Fig. 12.

To better illustrate the differences between males and females, we compare the occlusion maps obtained for these subgroups in ADHD cases. We show in Fig. 15 maps for the age group, specifically, diurnal activity for secondary subgroup and nocturnal activity for primary subjects; the figure reveals that primary females diagnosed with ADHD present less temporal dispersion for nocturnal activity compared to males. Moreover, there is a slight shift towards lower frequencies observed within that interval. Additionally, a lower dispersion of frequencies can be observed in the SF subgroup when compared to the SM subgroup.

The subgroup analysis conducted thus far has yielded valuable insights into the impact of age and gender on the pathology, as evident from the distinct patterns exhibited by each subgroup. The visual information we have introduced in the paper provides the physician with tools that can be used in clinical practice to explain the patient and their family the outcome of the automated diagnosis procedure as well as the location of the patient within those parameter spaces. The information is supported by quantitative indices obtained from the GMM that can be used to find physiologically explainable normality intervals. This makes the deep learning solution developed in [8] more explainable and, hence, more reliable.

Through the completion of this study, we have been able to explain differences in the measurable patterns of ADHD across different age and gender subgroups. This has facilitated the association of specific manifestations of the pathology with distinct patterns observed in the occlusion maps. Even though the results presented in this study provide valuable insight, and related statistics provide useful graphical information that may be even used in clinical practice, limitations in terms of the children study group should be acknowledged, specially for the secondary and female groups, where the number of patients is much lower. However, our dataset reveals the prevalence of this pathology in terms of age and gender. As individuals age, it is highly uncommon for patients without any medication to seek a clinician initial diagnosis. Conversely, it would pose ethical concerns that medication for diagnosed patients in their early years was deliberately delayed for the purpose of our experiment. Regarding gender, the prevalence of the pathology is notably lower in girls, resulting in fewer female patients being enrolled accordingly. Given the inherent challenges in recruiting

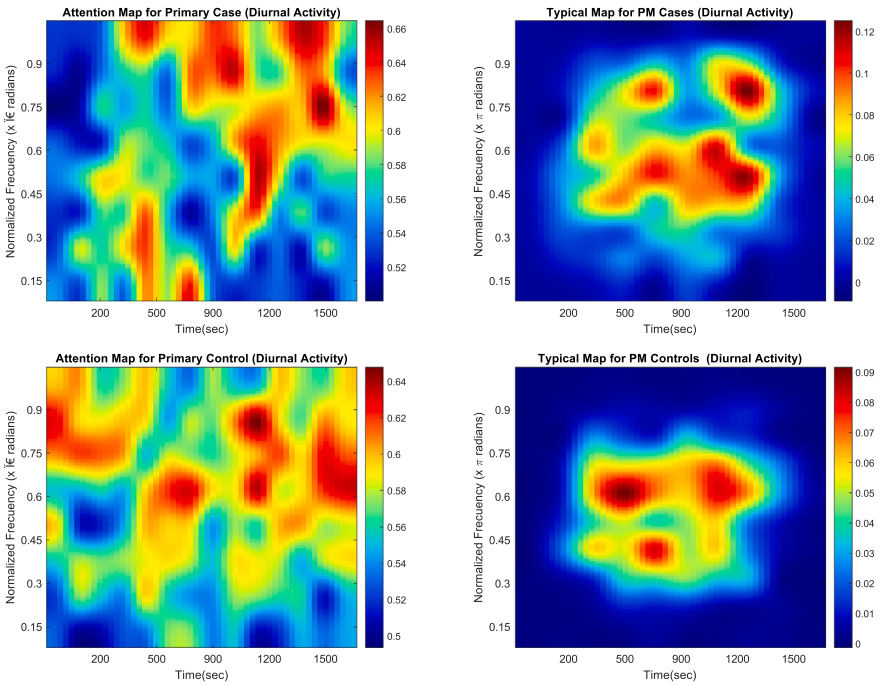

Fig. 14. Maps obtained for the Male cases (upper) and Male controls (lower), for the primary-diurnal CNN. Rightmost images are the attention maps, while leftmost images represent the occlusion maps.

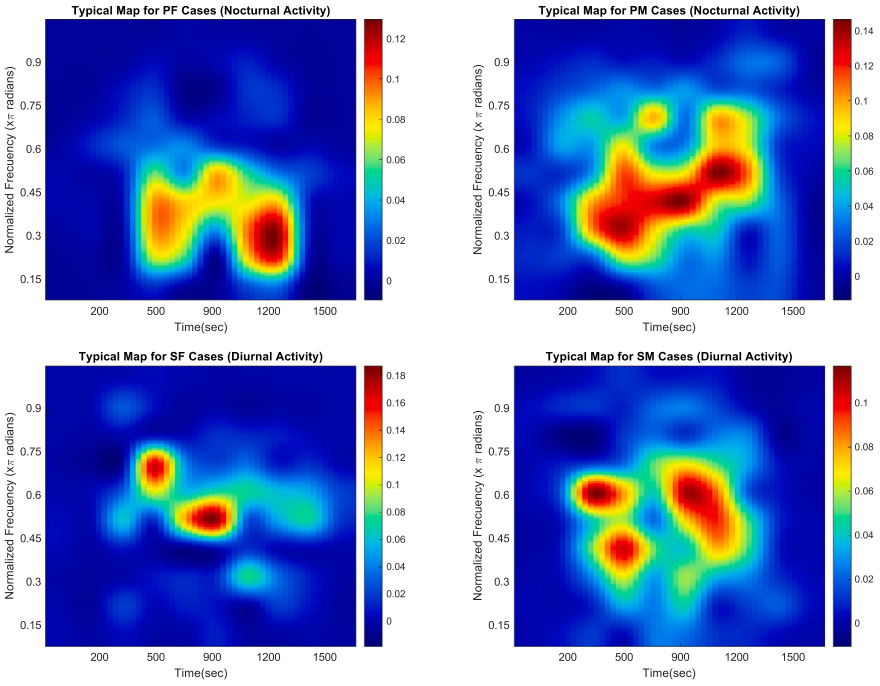

Fig. 15. Leftmost images: occlusion Maps obtained for the Primary Female cases (top) and Secondary female cases (bottom) for the female-nocturnal and female-diurnal CNN respectively. Rightmost images: maps obtained for Primary Male cases (top) and Secondary Male (bottom) cases for the male-nocturnal and male-diurnal CNN.

subjects for certain subgroups, one potential avenue to explore is the utilization of generative models.

6. Conclusion

In this work we have shown the presence of gender and age-related differences in individuals diagnosed with ADHD through the utilization of CNN visualization techniques, specifically, occlusion maps. We have developed a statistics-based quantification tool for these maps based on a Gaussian Mixture Model fit and hypothesis tests on its estimated parameters. Our methodology provides physicians with a valuable tool for comprehending the underlying movement patterns in objectively diagnosed ADHD children using AI. This work constitutes a step forward in achieving explainable AI for diagnosis support, unveiling new applications so far hindered by black box systems.

Declaration of competing interest

The authors declare no conflict of interest.

Acknowledgments

This work was supported in part by the Agencia Estatal de Investigación, and under Grants PID2020-115339RB-I00, TED2021-130090B-I00 and TED2021-131536B-I00, and by the company ESAOTE Ltd through grant 18IQBM. The last funder was not involved in the study design, collection, analysis, interpretation of data, the writing of this article, or the decision to submit it for publication. The work was also partly supported by the EU Horizon 2020 Research and Innovation Programme under the Marie Sklodowska-Curie grant agreement No 101008297. This article reflects only the authors' view. The European Union Commission is not responsible for any use that may be made of the information it contains.

References

[1] American Psychiatric Association c. Diagnostic and statistical manual of mental disorders : DSM-5. fifth ed.. VA: American Psychiatric Association Arlington; 2013, xliv, 947 p.
[2] Sayal K, Prasad V, Daley D, Ford T, Coghill D. ADHD in children and young people: prevalence, care pathways, and service provision. Lancet Psychiatry 2018;5(2):175–86.
[3] Rodríguez-Molinero L, López-Villalobos JA, Garrido-Redondo M, Sacristán-Martín AM, Martínez-Rivera MT, Ruiz-Sanz F. Estudio psicoclínico de prevalencia y comorbilidad del trastorno por déficit de atención con hiperactividad en Castilla y León (España). Pediatr Aten Primaria 2009;11:251–70.
[4] López Villalobos JA, Andrés de Llano JM, López Sánchez MV, Rodríguez Molinero L, Garrido Redondo M, Sacristán Martín AM, et al. Criterion validity and clinical usefulness of attention deficit hyperactivity disorder rating scale IV in attention deficit hyperactivity disorder (ADHD) as a function of method and age. Psicothema 2017;29(1):103–10.
[5] Ramtekkar UP, Reiersen AM, Todorov AA, Todd RD. Sex and age differences in attention-deficit/hyperactivity disorder symptoms and diagnoses: implications for DSM-V and ICD-11. J Am Acad Child Adolesc Psychiatry 2010;49(3):217–28.
[6] Hobbs N. Effects of under-diagnosis of attention deficit hyperactivity disorder in female students. 2019.
[7] Wasserstein J. Diagnostic issues for adolescents and adults with ADHD. J Clin Psychol 2005;61(5):535–47.
[8] Amado-Caballero P, Casaseca-de-la Higuera P, Alberola-Lopez S, Andrés-de Llano JM, López-Villalobos JA, Garmendia-Leiza JR, et al. Objective ADHD diagnosis using convolutional neural networks over daily-life activity records. IEEE J Biomed Health Inform 2020;24(9):2690–700.
[9] Staller J, Faraone SV. Attention-deficit hyperactivity disorder in girls. CNS Drugs 2006;20(2):107–23.
[10] Rosch KS, Mostofsky SH, Nebel MB. ADHD-related sex differences in fronto-subcortical intrinsic functional connectivity and associations with delay discounting. J Neurodev Disord 2018;10(1):1–14.
[11] Murray AL, Booth T, Eisner M, Auyeung B, Murray G, Ribeaud D. Sex differences in ADHD trajectories across childhood and adolescence. Dev Sci 2019;22(1):e12721.
[12] Mowlem FD, Rosenqvist MA, Martin J, Lichtenstein P, Asherson P, Larsson H. Sex differences in predicting ADHD clinical diagnosis and pharmacological treatment. Eur Child Adolesc Psychiatry 2019;28(4):481–9.
[13] Mowlem F, Agnew-Blais J, Taylor E, Asherson P. Do different factors influence whether girls versus boys meet ADHD diagnostic criteria? Sex differences among children with high ADHD symptoms. Psychiatry Res 2019;272:765–73.
[14] Ingram S, Hechtman L, Morgenstern G. Outcome issues in ADHD: Adolescent and adult long-term outcome. Ment Retard Dev Disabil Res Rev 1999;5(3):243–50.
[15] Becker SP, Lienesch JA. Nighttime media use in adolescents with ADHD: Links to sleep problems and internalizing symptoms. Sleep Med 2018;51:171–8.
[16] Becker SP, Langberg JM, Eadeh H-M, Isaacson PA, Bourchtein E. Sleep and daytime sleepiness in adolescents with and without ADHD: Differences across ratings, daily diary, and actigraphy. J Child Psychol Psychiatry 2019;60(9):1021–31.
[17] Ward AR, Sibley MH, Musser ED, Campez M, Bubnik-Harrison MG, Meinzer MC, et al. Relational impairments, sluggish cognitive tempo, and severe inattention are associated with elevated self-rated depressive symptoms in adolescents with ADHD. ADHD Atten Defic Hyperact Disord 2019;11(3):289–98.
[18] Powell V, Riglin L, Hammerton G, Eyre O, Martin J, Anney R, et al. What explains the link between childhood ADHD and adolescent depression? Investigating the role of peer relationships and academic attainment. Eur Child Adolesc Psychiatry 2020;29(11):1581–91.
[19] Zou L, Zheng J, Miao C, Mckeown MJ, Wang ZJ. 3D CNN based automatic diagnosis of attention deficit hyperactivity disorder using functional and structural MRI. IEEE Access 2017;5:23626–36.
[20] Wang T, Kamata S-i. Classification of structural MRI images in ADHD using 3D fractal dimension complexity map. In: 2019 IEEE international conference on image processing. IEEE; 2019, p. 215–9.
[21] Khullar V, Salgotra K, Singh HP, Sharma DP. Deep learning-based binary classification of ADHD using resting state MR images. Augment Hum Res 2021;6(1):1–9.
[22] Riaz A, Asad M, Alonso E, Slabaugh G. DeepFMRI: End-to-end deep learning for functional connectivity and classification of ADHD using fMRI. J Neurosci Methods 2020;335:108506.
[23] Chauhan N, Choi B-J. DNN based classification of ADHD fMRI data using functional connectivity coefficient. Int J Fuzzy Log Intell Syst 2020;20(4):255–60.
[24] Kim B, Park J, Kim T, Kwon Y. Finding essential parts of the brain in rs-fMRI can improve diagnosing ADHD by deep learning. 2021, arXiv preprint arXiv:2108.10137.
[25] Mao Z, Su Y, Xu G, Wang X, Huang Y, Yue W, et al. Spatio-temporal deep learning method for ADHD fMRI classification. Inform Sci 2019;499:1–11.
[26] Ke H, Wang F, Ma H, He Z. ADHD identification and its interpretation of functional connectivity using deep self-attention factorization. Knowl-Based Syst 2022;250:109082.
[27] Chen Y, Gao Y, Jiang A, Tang Y, Wang C. ADHD classification combining biomarker detection with attention auto-encoding neural network. Biomed Signal Process Control 2023;84:104733.
[28] Dong Q, Qiang N, Lv J, Li X, Liu T, Li Q. Spatiotemporal attention autoencoder (STAAE) for ADHD classification. In: Medical image computing and computer assisted intervention–MICCAI 2020: 23rd international conference, Lima, Peru, October 4–8, 2020, proceedings, part VII 23. Springer; 2020, p. 508–17.
[29] Zhang T, Li C, Li P, Peng Y, Kang X, Jiang C, et al. Separated channel attention convolutional neural network (SC-CNN-attention) to identify ADHD in multi-site rs-fMRI dataset. Entropy 2020;22(8):893.
[30] Qiang N, Dong Q, Liang H, Ge B, Zhang S, Zhang C, et al. A novel ADHD classification method based on resting state temporal templates (RSTT) using spatiotemporal attention auto-encoder. Neural Comput Appl 2022;34(10):7815–33.
[31] Chen H, Song Y, Li X. A deep learning framework for identifying children with ADHD using an EEG-based brain network. Neurocomputing 2019;356:83–96.
[32] Ahmadi A, Kashefi M, Shahrokhi H, Nazari MA. Computer aided diagnosis system using deep convolutional neural networks for ADHD subtypes. Biomed Signal Process Control 2021;63:102227.
[33] Vahid A, Bluschke A, Roessner V, Stober S, Beste C. Deep learning based on event-related EEG differentiates children with ADHD from healthy controls. J Clin Med 2019;8(7):1055.
[34] Chen H, Song Y, Li X. Use of deep learning to detect personalized spatial-frequency abnormalities in EEGs of children with ADHD. J Neural Eng 2019;16(6):066046.
[35] Li Y, Yang H, Li J, Chen D, Du M. EEG-based intention recognition with deep recurrent-convolution neural network: Performance and channel selection by Grad-CAM. Neurocomputing 2020;415:225–33.
[36] Moghaddari M, Lighvan MZ, Danishvar S. Diagnose ADHD disorder in children using convolutional neural network based on continuous mental task EEG. Comput Methods Programs Biomed 2020;197:105738.
[37] Dubreuil-Vall L, Ruffini G, Camprodon JA. Deep learning convolutional neural networks discriminate adult ADHD from healthy individuals on the basis of event-related spectral EEG. Front Neurosci 2020;251.
[38] Bakhtyari M, Mirzaei S, Amiri H. Combination of ConvLSTM and attention mechanism to diagnose ADHD based on EEG signals. In: 2021 7th international conference on signal processing and intelligent systems. IEEE; 2021, p. 1–5.
[39] Muñoz-Organero M, Powell L, Heller B, Harpin V, Parker J. Automatic extraction and detection of characteristic movement patterns in children with ADHD based on a convolutional neural network (CNN) and acceleration images. Sensors 2018;18(11):3924.
[40] O'Mahony N, Florentino-Liano B, Carballo JJ, Baca-García E, Rodríguez AA. Objective diagnosis of ADHD using IMUs. Med Eng Phys 2014;36(7):922–6.
[41] Kaur A, Kahlon KS. Accurate identification of ADHD among adults using real-time activity data. Brain Sci 2022;12(7):831.
[42] Mordvintsev A, Olah C, Tyka M. Inceptionism: Going deeper into neural networks. 2015, Google Research https://research.googleblog.com/2015/06/inceptionism-going-deeper-into-neural.html.
[43] Zhou B, Khosla A, Lapedriza A, Oliva A, Torralba A. Learning deep features for discriminative localization. In: Proceedings of the IEEE conference on computer vision and pattern recognition. 2016, p. 2921–9.
[44] Selvaraju RR, Cogswell M, Das A, Vedantam R, Parikh D, Batra D. Grad-cam: Visual explanations from deep networks via gradient-based localization. In: Proceedings of the IEEE international conference on computer vision. 2017, p. 618–26.
[45] Zeiler MD, Fergus R. Visualizing and understanding convolutional networks. In: European conference on computer vision. Springer; 2014, p. 818–33.

[46] DuPaul GJ, Power TJ, Anastopoulos AD, Reid R. ADHD rating Scale—IV: Checklists, norms, and clinical interpretation. Guilford Press; 1998.
[47] Kampa K, Hasanbelliu E, Principe JC. Closed-form Cauchy-Schwarz PDF divergence for mixture of Gaussians. In: The 2011 international joint conference on neural networks. IEEE; 2011, p. 2578–85.
[48] Woo S, Park J, Lee J-Y, Kweon IS. Cbam: Convolutional block attention module. In: Proceedings of the European conference on computer vision. (ECCV), 2018, p. 3–19.
[49] Szentkirályi A, Madarász CZ, Novák M. Sleep disorders: impact on daytime functioning and quality of life. Expert Rev Pharm Outcomes Res 2009;9(1):49–64.